
DETAILS ENHANCEMENT IN UNSIGNED DISTANCE FIELD LEARNING FOR HIGH-FIDELITY 3D SURFACE RECONSTRUCTION

A PREPRINT

Cheng Xu

Institute of Software,
Chinese Academy of Sciences

Fei Hou*

Institute of Software,
Chinese Academy of Sciences

Wencheng Wang

Institute of Software,
Chinese Academy of Sciences

Hong Qin

Department of Computer Science,
Stony Brook University

Zhebin Zhang

InnoPeak Technology

Ying He

S-Lab
Nanyang Technological University

June 4, 2024

ABSTRACT

While Signed Distance Fields (SDF) are well-established for modeling watertight surfaces, Unsigned Distance Fields (UDF) broaden the scope to include open surfaces and models with complex inner structures. Despite their flexibility, UDFs encounter significant challenges in high-fidelity 3D reconstruction, such as non-differentiability at the zero level set, difficulty in achieving the exact zero value, numerous local minima, vanishing gradients, and oscillating gradient directions near the zero level set. To address these challenges, we propose Details Enhanced UDF (DEUDF) learning that integrates normal alignment and the SIREN network for capturing fine geometric details, adaptively weighted Eikonal constraints to address vanishing gradients near the target surface, unconditioned MLP-based UDF representation to relax non-negativity constraints, and a UDF-tailored method for extracting iso-surface with non-constant iso-values. These strategies collectively stabilize the learning process from unoriented point clouds and enhance the accuracy of UDFs. Our computational results demonstrate that DEUDF outperforms existing UDF learning methods in both accuracy and the quality of reconstructed surfaces. We will make the source code publicly available.

1 Introduction

While signed distance fields (SDF) are favored for their capability to represent watertight surfaces, unsigned distance fields (UDF) provide a means to model both open surfaces and objects with complex inner structures. However, achieving high-quality UDFs that accurately reconstruct 3D surfaces with fine geometric details is challenging for several reasons. Firstly, UDFs struggle to precisely achieve a zero value, making it difficult to identify the exact surface boundaries. Secondly, UDFs are theoretically non-differentiable at the zero level set, resulting in vanishing gradients near the target surface. This issue leads to numerous undesired local minima, complicating the extraction of the zero level set. Thirdly, the gradient directions of UDFs tend to oscillate near the surface, causing the reconstructed surfaces to be fragmented [1].

Due to the inherently low accuracy of learned UDFs, the extracted zero level sets are typically over-smoothed and lack crucial geometric details. Several studies have aimed to enhance the precision of UDF learning. For instance, NDF [2] trains a shape encoder and a decoder from 3D surfaces of various types, including point clouds, meshes and mathematical functions. As a supervised method, its performance heavily relies on the quality and diversity of the training dataset. Unsupervised approaches, such as CAP-UDF [3] and LevelSetUDF [4], offer greater flexibility in handling a wider range of 3D models. Despite advancements in UDF learning techniques, all existing methods

*Corresponding author: F. Hou (houfei@ios.ac.cn)

still suffer from relatively low accuracy in the learned distance fields compared to SDFs. This limitation significantly diminishes their practical usage in real-world applications.

This paper introduces a new method, called Details Enhanced UDF (DEUDF) learning, aimed at enhancing the accuracy of UDF learning from unoriented point clouds to ensure that learned UDFs can capture the fine geometric details of target surfaces. A key observation is the significant role normal directions play in learning fine details. Although obtaining globally consistent orientations is challenging due to its combinatorial and global optimization nature, acquiring normal directions locally, for instance, through principal component analysis [5], is feasible. Consequently, we constrain the UDF gradients to align with normal directions to enhance detail capture, while disregarding normal orientations.

To overcome the limitation of UDFs not achieving the exact zero value, we relax the strict requirements that UDFs must be non-negative and that the surface must precisely correspond to the zero iso-surfaces. This adaptation enables the use of an unconditioned multilayer perceptron (MLP) meaning an MLP that outputs its value directly without any additional operations to make the output positive. Unlike traditional methods that generate UDFs by taking the absolute value of a learned SDF [4] – prone to inducing oscillating gradients – or by using the softplus activation function in MLPs to eliminate negative values [6] – leading to vanishing gradients – our relaxation not only addresses the vanishing gradients but also stabilizes the oscillation of gradient directions near the surface.

While SDFs maintain well-behaved gradients with consistent unit length throughout 3D space, UDFs often experience vanishing gradients at the zero level set, diminishing the effectiveness of uniformly applied Eikonal constraints for UDF learning. To address this issue, we propose an adaptively weighted Eikonal constraint, specifically tailored to align with the unique properties of UDFs. Moreover, we incorporate the SIREN network [7] to represent high-frequency details in UDFs, thereby enhancing the encoding capabilities of our model. We consider the local minimum around zero – both positive and negative – as the intended surface and adopt DCUDF [8], an optimization-based iso-surfacing algorithm, to extract the iso-surface with non-constant iso-values.

By integrating normal alignment, unconditioned MLPs with SIREN activation functions, adaptively weighted Eikonal constraints, and UDF-tailored iso-surfacing techniques, DEUDF significantly improves the accuracy of UDF learning. Evaluations on benchmark datasets demonstrate our method outperforms baseline methods in terms of UDF accuracy and quality of reconstructed surfaces.

2 Related work

Surface reconstruction from point clouds has been studied extensively for the last three decades. The field has seen significant evolution, from computational geometry methods [9, 10] to implicit function techniques [5, 11, 12, 13], and more recently to deep learning approaches [14, 2, 4, 15, 16, 17]. Due to space constraints, this section primarily focuses on deep learning-based 3D reconstruction techniques.

Both signed distance fields and occupancy fields effectively represent closed surfaces. An occupancy field defines whether each point in space is inside or outside a given shape. ONet [18] employs a deep neural network classifier to implicitly represent 3D surfaces as a continuous decision boundary, while IF-Net [19] and CONet [20] use encoders to capture shape. Compared to occupancy fields, SDFs provide additional information about the distance of a point from the surface of the object, making them favored for applications that require accurate shape representation, such as reconstruction, shape interpolation and completion. DeepSDF [14] introduces an innovative implicit encoder that defines the boundary of a 3D shape as the zero level set of a learned implicit function. Following this, numerous neural SDF-based works have been developed. For example, DeepLS [21] utilizes a grid structure to store latent codes for local shape features, SIREN [7] introduces a novel activation function for increasing the network’s capability to capture high-frequency signals, and IDF [22] employs displacement maps to enhance the representation of fine details. Additionally, SDFs have been utilized to represent geometric shapes for neural rendering tasks, such as NeuS[23] and VolSDF [24], which leverage SDFs for 3D reconstruction from multi-view images.

To model general non-watertight surface, Chibane et al. [2] introduced neural unsigned distance fields, which predict the unsigned distance from a query point to the nearest surface point. GIFS [25] models the relationship between points rather than between points and surfaces, while NVF [26] learns a vector as an alternative to calculating gradient from UDFs, representing the direction from query points to the target surface. Unlike these methods, which utilize separate neural networks to extract supplementary information that aids UDF learning, CAP-UDF [3] and GeoUDF [15] focus on enhancing the density of the input point clouds via adopting upsampling techniques. Despite these advancements, the challenge of ambiguous gradients near the zero level set remains, due to the non-differentiability of UDFs at this juncture. To address this challenge, LevelSetUDF[4] introduces constraints between non-differentiable zero level set and differentiable non-zero level set, while DUDF [17] adopts a new representation to maintain differentiability

at points close to the target surface. Although LevelSetUDF and DUDF tackle the non-differentiable issues, they still struggle to match the quality of reconstruction—particularly for surfaces with fine details—achieved SDF learning methods. Additionally, similar to SDFs, UDFs are also utilized to implicitly represent 3D shapes in neural rendering tasks, such as 3D reconstruction and novel view synthesis from multi-view images [27, 6, 28]. See Table 1 for a qualitative comparison of existing UDF learning methods.

Extracting the zero level set from UDFs is technically non-trivial, as it is rare for the learned UDFs to precisely reach zero values. There are several research efforts aiming at addressing this issue. Gradient-based methods such as CAP-UDF [3], MeshUDF [1] and GeoUDF [15] use both gradient directions and UDF values to detect zero crossings, while optimization-based techniques, such as DCUDF [8], focus on identifying local minima within the input UDFs.

Table 1: Qualitative comparison of existing UDF learning methods. HS: hyperbolic scaling; PE: positional encoding; ABS: absolute value.

Method	Input	MLP	Eikonal	Non-negativity	Learning
NeUDF	multi-view images	softplus+PE	uniform	softplus	unsupervised
NeuralUDF	multi-view images	softplus+PE	uniform	ABS	unsupervised
2S-UDF	multi-view images	softplus+PE	uniform	softplus	unsupervised
NDF	sparse point clouds	ReLU	-	ABS	supervised
GIFS	sparse point clouds	ReLU	-	ABS	supervised
GeoUDF	sparse point clouds	LeakyReLU	-	ABS	supervised
DUDF	dense point clouds	SIREN	uniform	ABS+HS	supervised
CAP-UDF	sparse point clouds	ReLU+PE	-	ABS	unsupervised
LevelSetUDF	dense point clouds	ReLU+PE	-	ABS	unsupervised
Ours	dense point clouds	SIREN	adaptive	no	unsupervised

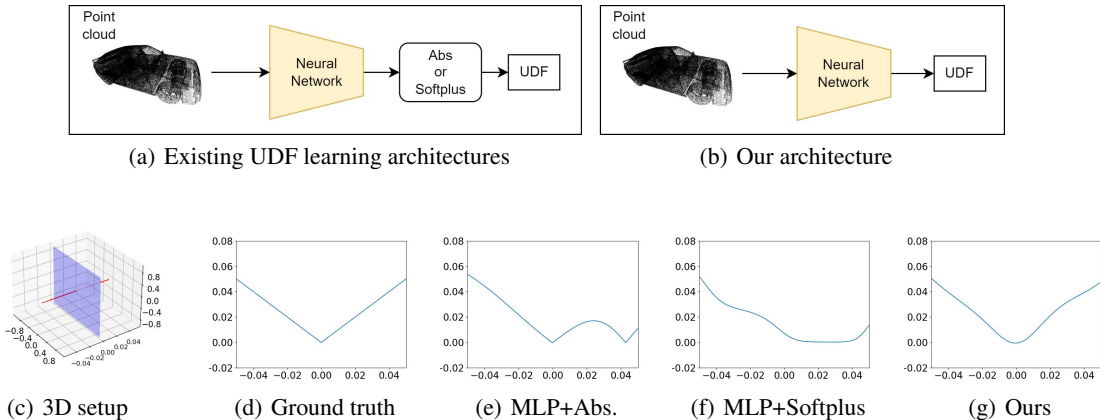


Figure 1: Illustration of UDF learning with various neural representations. (a) Existing neural network architectures often use an absolute value or softplus function to prevent negative distances. (b) In contrast, our method relaxes the non-negative condition and employs an unconditioned MLP with the SIREN activation function for predicting the distances. (c) To show the differences between existing representations and ours, we consider a plane π and a line perpendicular to π . Points along this line, as they pass through the plane, are used to plot the unsigned distance, shown in (d)-(g). The horizontal axis represents a signed distance range from -0.05 to 0.05, while the vertical axis measures the unsigned distance. Ideally, the unsigned distance should exhibit a perfect “V” shape relative to the signed distance, as shown in (d). However, UDFs parameterized by conditioned MLPs can present defects. For example, learning an SDF followed by taking the absolute value results in a “W”-shaped distance field around the zero level set (e). Employing the softplus activation function to eliminate negative values yields learned UDFs with vanishing gradients across a relatively large distance range near the zero value (f). In contrast, our method, which employs unconditioned MLPs, significantly narrows this range of vanishing gradients (g).

3 Method

Let $\mathcal{P} = \{\mathbf{p}_i \in \mathbb{R}^3\}_{i=1}^n$ represent the input raw point cloud, which has been uniformly scaled to fit within the cube domain $\Omega = [-1, 1]^3$. We employ an MLP to parameterize the UDF for \mathcal{P} , denoted by f . Our objective is to accurately learn f in order to extract a high-fidelity mesh that represents the geometric structure of \mathcal{P} .

3.1 Relaxation of non-negative constraints

Traditional methods for learning UDFs generally ensure non-negative distance values by adopting specific strategies, such as taking the absolute value or using the softplus in the last layer. However, as illustrated in Figure 1, these approaches have significant drawbacks in accurately representing distances near zero. For example, using the absolute value results in UDFs exhibiting a “W” shape, leading to changes in gradient directions and the presence of multiple minimum values. Moreover, when the absolute value is applied to an SDF, the resulting UDF exhibits characteristics similar to those of an SDF. This leads to the unintended consequence of gap filling even in point clouds that represent open surfaces. See Figure 3 for an example. On the other hand, employing the softplus activation function helps avoid the W-shaped artifacts associated with the absolute value approach. Nonetheless, this method tends to generate a U-shaped distance field, characterized by a relatively wide bandwidth around the zero value, approximately between 0 and 0.04. This occurs because for $x \in (-\infty, 0)$, $\text{softplus}(x)$ yields a small positive value with almost zero derivatives. Consequently, this results in vanishing gradients for query points near the target surface, which can significantly hinder the effectiveness of network training that relies on gradient-based optimization techniques.

Observing both vanishing gradients and oscillating gradient directions stem from the strict non-negative constraint on distance values, we propose relaxing the conditions that require UDFs to be non-negative and the surface to coincide precisely with zero iso-surface. We use unconditioned MLPs to represent UDFs and consider the local minimum of the UDF value around zero, which may be either positive or negative, as the point through which the intended surface passes. As illustrated in Figure 1 (e), this relaxation results in a distance function with a significantly narrower bandwidth compared to using the softplus activation function, thereby providing a high-quality approximation to the ground truth distance field, which exhibits a V-shaped profile.

With UDFs parameterized by unconditioned MLPs, we define the following loss functions for learning UDFs without ground-truth supervision:

$$\mathcal{L}_{\text{dist}} = \sum_{\mathbf{p}_i \in \mathcal{P}} |f(\mathbf{p}_i)|, \quad (1)$$

and

$$\mathcal{L}_{\text{positive}} = \sum_{\mathbf{x} \in \Omega} \exp(-100f(\mathbf{x})). \quad (2)$$

The distance term $\mathcal{L}_{\text{dist}}$ encourages the zero level set of the learned UDFs to pass through the input points \mathbf{p}_i . The positivity enforcement term $\mathcal{L}_{\text{positive}}$ is designed to ensure that values of $f(\mathbf{x})$ for off-surface points \mathbf{x} are large and positive. This term encourages the majority of sample points are assigned positive values, effectively preventing the generation of negative distance values and ensuring the function behaves like a true UDF. Additionally, it helps to maintain a clear distinction between surface and non-surface regions, crucial for accurate surface reconstruction.

Remark. In NeuralUDF [27], a similar loss term in the form $\exp(-100|f|)$ was used. It is important to note that our loss term does not include the absolute value. This subtle difference significantly impacts the behavior of the learned distance field f . With the absolute value, their loss encourages $|f|$ being a large positive value, which consequently reduces the occurrence of points with zero distance values. This reduction minimizes the presence of small disconnected components in the reconstructed surfaces [22, 27]. Therefore, the \exp in their loss functions acts as a regularizer to smooth the learned distance fields. As mentioned above, the use of the absolute value $|f|$ in the loss function can lead to undesired side effects, such as a W-shaped profile in the learned UDFs, which may consequently result in watertight models. In sharp contrast, our loss term, which omits the absolute value, serves as a soft non-negative constraint. This encourages f to remain positive as much as possible, thus differentiating it from an SDF, and enabling f to mimic a true UDF. Even though DCUDF [8] used an unconditional MLP to represent UDF, it needs the ground truth UDF for supervision. Otherwise, it cannot learn the UDF.

3.2 Normal alignment

Normal directions are critical for enhancing surface details in the reconstruction process. Let $\mathcal{N} = \{\mathbf{n}_i\}_{i=1}^n$ represent the set of unit normals for the point set \mathcal{P} . Following [5], we apply principal component analysis to each point \mathbf{p}_i to

determine its normal direction \mathbf{n}_i . Since UDF gradients typically vanish on the surface, it is impractical to directly constrain the gradients of \mathcal{P} .

To address this issue, we generate a sample point set $\mathcal{Q} = \{\mathbf{q}_i\}_{i=1}^n$ in each training epoch, where each point \mathbf{q}_i is strategically displaced from the surface. Specifically, $\mathbf{q}_i = \mathbf{p}_i + \lambda_i \mathbf{n}_i$, with the displacement λ_i randomly chosen from the ranges $[-0.003, 0]$ and $[0, 0.003]$, respectively. This ensures that \mathcal{Q} contains samples on both sides of the surface, enabling a balanced evaluation of regions close to the geometric structure of interest. We then impose constraints on the UDF gradient directions at points in \mathcal{Q} , calculated using the following normal alignment loss term:

$$\mathcal{L}_{\text{normal}} = \sum_{\mathbf{q}_i \in \mathcal{Q}, \mathbf{n}_i \in \mathcal{N}} \left(1 - \frac{\nabla f(\mathbf{q}_i) \cdot \mathbf{n}_i}{\|\nabla f(\mathbf{q}_i)\|_2 \cdot \|\mathbf{n}_i\|_2} \text{sign}(\lambda_i) \right). \quad (3)$$

3.3 Adaptively weighted Eikonal constraints

The Eikonal constraint, expressed as $\|\nabla f\| = 1$, is extensively utilized in the learning processes for SDFs. However, when applied to UDFs, this approach faces challenges due to the diminished gradient magnitudes near the zero level set. Direct application of Eikonal constraints to regularize UDFs may cause the actual surface to deviate from the input point cloud \mathcal{P} and may also increase the minima of the learned UDF, as illustrated in Table 3 and Figure 4. To address this issue, we propose a formulation for an adaptively weighted Eikonal loss term:

$$\mathcal{L}_{\text{eikonal}} = \sum_{\mathbf{x} \in \mathcal{Q} \cup \Omega} \delta(f(\mathbf{x})) \left| \|\nabla f(\mathbf{x})\|_2 - 1 \right|, \quad (4)$$

where the weight function, $\delta(\cdot)$, is designed to reduce the contribution from points close to the target surface. A U-shaped function with controllable bandwidth serves this purpose effectively. In our implementation, we employ the attenuation function used in IDF [22] as our weight as $\delta(d) = \left(1 + \left(\frac{\xi}{d}\right)^4\right)^{-1}$, where ξ represents the threshold beyond which the influence of the Eikonal constraint begins to diminish significantly. In our experiments, we initially set ξ to 0.01 and gradually decrease ξ to 0.002 over the course of the learning process, following the learning rate. This adjustment is made to enhance the attenuation effect. We evaluate the Eikonal loss $\mathcal{L}_{\text{eikonal}}$ for points in the set \mathcal{Q} , which serves as a proxy of the target geometry, as well as for randomly sampled points throughout the entire domain Ω .

3.4 UDF learning

For the network architecture, we employ a 5-layer SIREN network [7], which consists of 256 units per layer. The network utilizes a sinusoidal activation function $\sin(\omega x)$, with a frequency parameter $\omega = 60$ in our implementation, to effectively encode high-frequency details. Our network takes spatial coordinates (x, y, z) as inputs and outputs the predicted unsigned distance.

The training process aims to minimize the following loss function:

$$\mathcal{L} = \lambda_1 \mathcal{L}_{\text{dist}} + \lambda_2 \mathcal{L}_{\text{positive}} + \lambda_3 \mathcal{L}_{\text{normal}} + \lambda_4 \mathcal{L}_{\text{eikonal}} \quad (5)$$

where λ_i s are weights assigned to balance the contributions from the four loss terms. We empirically set $\lambda_1 = 400$, $\lambda_2 = 50$, $\lambda_3 = 40$ and $\lambda_4 = 10$ in our implementation. We train the neural network using the Adam [29] optimizer, starting with a learning rate of 0.00005. The learning rate decays to zero following a cosine annealing[30] schedule.

3.5 Isosurface extraction

After obtaining the UDFs, we proceed to extract the iso-surface from the learned UDFs. Due to the relaxation of the non-negative constraints, the target geometry does not align precisely with the zero level set. Instead, we identify the target surface as the one passing through the local minima (which can be either positive or negative) of the UDFs near the zero values.

One possible method for extracting the target geometry from UDFs involves explicitly using the UDF gradient, such as MeshUDF [1] and GeoUDF [15], both of which are variants of the standard Marching Cubes algorithm. On each cube edge, if the gradient directions of the UDF at the two endpoints are opposite and their UDF values are below a specified threshold, a zero crossing is marked on that edge. However, this approach is not suitable for our purpose because our learned UDFs do not ensure the positivity of the distance value, and the local minima may exceed the specified UDF threshold. If this occurs, the iso-surfacing method would exclude these cubes, leading to the creation of extracted surfaces with undesired holes.

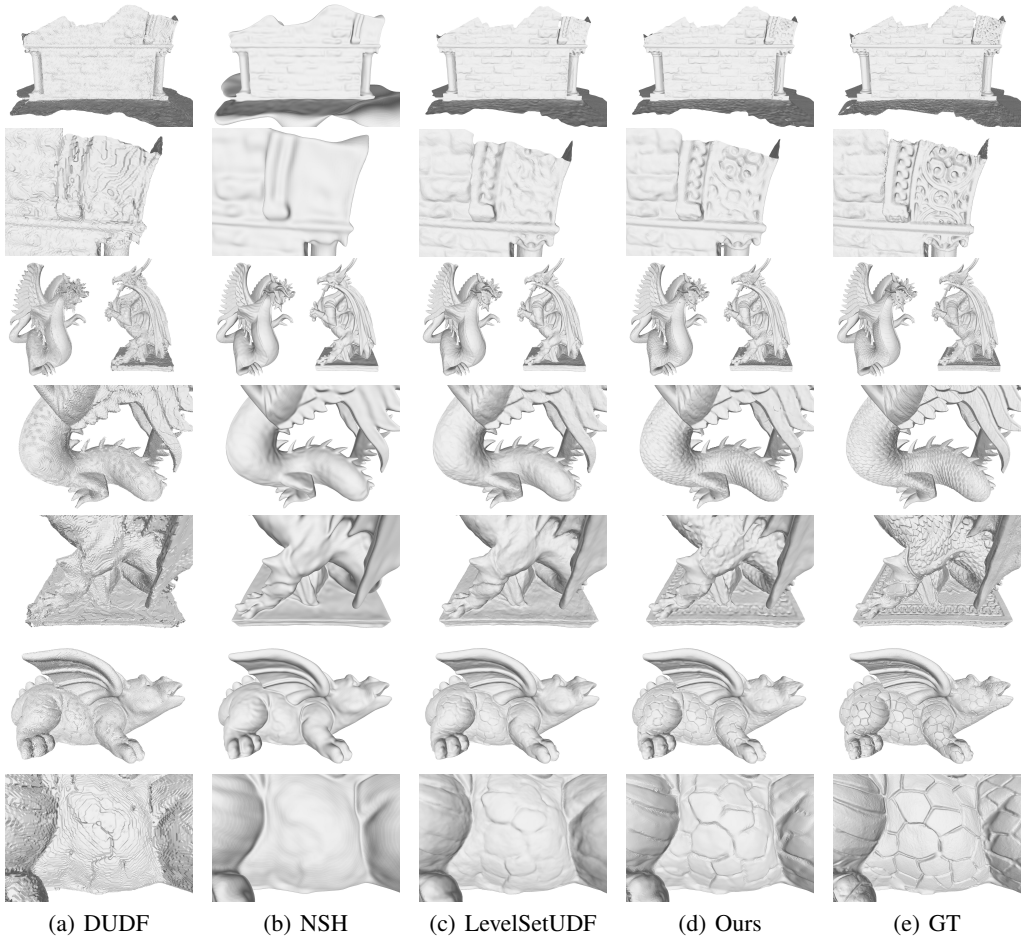


Figure 2: Visual comparison with two recent UDF learning approaches, DUDF [17] and LevelSetUDF [4], and one recent SDF learning method, NSH [31], on surfaces with fine geometric details. Our method yields visually pleasing results, reconstructing significantly more details than the other methods.

To tackle this challenge, we adopt the optimization-based method DCUDF [8], which initiates by extracting a double cover using the Marching Cubes algorithm at a small positive iso-value on the UDF. Subsequently, it shrinks the double cover to the local minimum of the UDF. This method does not require the UDF to be strictly positive nor does it depend on a threshold to select candidate cubes. As a result, it effectively identifies the local minima, yielding a high-quality triangle mesh that accurately represents the target surface.

4 Experiments

4.1 Datasets

We evaluate our method using three datasets: ShapeNet-Cars [32] with 108 models (We select all models named starting with “1”), the Stanford 3D Scene Dataset [33] with 5 models and the Stanford 3D Scan Repository ² with 8 models. For each shape, we randomly sample 300K points as input. After learning the UDFs, we employ DCUDF with a resolution of 512^3 to extract the target surface. To evaluate the accuracy, We use Chamfer distance (CD) and F-score as quantitative measures. For F-score, we set the thresholds to 0.01 and 0.005. Following previous methods [3, 4], we randomly sample 100K points from both the reconstructed surfaces and the ground truth meshes for computing CD and F-score. We report our results on an NVIDIA Tesla V100 GPU with 32GB memory (about 5GB used for a UDF learning). It takes about 30 minutes to learn a UDF.

²<https://graphics.stanford.edu/data/3Dscanrep/>

4.2 Results & comparisons

We compare our method with three state-of-the-art UDF learning methods: LevelSetUDF [4], CAP-UDF [3] and DUDF[17]. Since we adopt DCUDF [8] for surface extraction, we also test DCUDF for the three baselines to ensure fairness of comparisons. For CAP-UDF [3] and LevelSetUDF [4], we observe that DCUDF could produce better results than their original implementations in terms of Chamfer distances and visual effects. But for DUDF, the results of DCUDF are not as good as the original results. Therefore, to report the best results of the baseline methods, we choose to adopt DCUDF for extracting the zero level set from the UDF outputs from both CAP-UDF and LevelSetUDF. While DUDF uses their original results for comparisons. For completeness, we also report the original results of CAP-UDF and LevelSetUDF in the supplementary material for visual and quantitative comparisons.

Additionally, we assess our approach against IDF [22] and NSH [31], two state-of-the-art SDF learning methods, on the watertight surfaces with fine geometric details from the Stanford 3D Scan Repository. See Table 2 and Figure 2.

3D objects with fine geometric details To explore the ability of our method for representing 3D objects with fine geometric details, we evaluate our method on Stanford 3D Scene dataset and Stanford 3D Scan dataset. As shown in Table 2 and Figure 2, our method achieves the best performance in UDF-based methods, and performs close to SDF-base methods.

3D objects with complex inner structures We further explore our method for representing 3D objects and scenes with complex inner structures. We evaluate our method on Stanford 3D Scene and ShapeNet-Cars datasets. As shown in Table 2 and Figure 3, our method is more stable on complex structures and performs optimally in the representation of open boundaries.

4.3 Ablation studies

We conduct ablation studies to demonstrate the effectiveness of each component within our method. The results are shown in Figure 4 and Table 3.

Table 2: Quantitative results on the Stanford 3D Scene Dataset, the Stanford 3D Scans (watertight) and ShapeNet-Cars. Chamfer distances are measured in the unit of $\times 10^{-3}$. We randomly sampled 100K points from each ground truth mesh and then computed both CDs and F-scores as reference performance metrics. Therefore, the closer the actual performance metrics are to these references, the higher the quality of the results produced by the method. For CAP-UDF and LevelSetUDF, following their official surface extraction implementations, we removed artifacts that are far from the ground truth point cloud after extracting the mesh by DCUDF.

Method	Distance	Stanford 3D Scene				Stanford 3D Scan				ShapeNet-Cars			
		Chamfer-L1 (\downarrow)		F-score (\uparrow)		Chamfer-L1 (\downarrow)		F-score (\uparrow)		Chamfer-L1 (\downarrow)		F-score (\uparrow)	
		Mean	Median	$F1^{0.01}$	$F1^{0.005}$	Mean	Median	$F1^{0.01}$	$F1^{0.005}$	Mean	Median	$F1^{0.01}$	$F1^{0.005}$
CAP-UDF	Unsigned	3.37	3.33	98.96	84.51	4.12	3.87	99.12	69.02	4.97	4.63	95.37	56.42
DUDF	Unsigned	3.79	3.26	97.33	79.43	4.20	3.95	99.07	68.10	6.05	5.51	89.02	44.18
LeverSetUDF	Unsigned	3.16	2.90	99.17	85.92	4.12	3.87	99.04	68.83	5.03	4.63	95.01	55.57
NSH	Signed	-	-	-	-	4.21	3.96	99.12	68.18	-	-	-	-
IDF	Signed	-	-	-	-	4.07	3.83	99.14	69.66	-	-	-	-
Ours	Unsigned	3.09	2.85	99.41	86.38	4.08	3.83	99.14	69.59	4.91	4.58	95.53	56.98

Unconditioned MLPs We assess the impact of using an unconditioned SIREN network on the performance of our method by comparing it to versions of the SIREN network that utilize absolute value and softplus function in the output layer, respectively. As shown in Table 3, the SIREN network with an absolute value output tends to learn a “fake” UDF, which behaves similarly to an SDF in modeling watertight models. On the other hand, due to the vanishing gradient effect of softplus, the reconstructed mesh using the SIREN network with a softplus output is typically over-smoothed.

Normal alignment To evaluate the contribution of normal alignment to reconstruct geometric details in our model, we performance comparisons between versions of our method with and without the normal alignment loss. The results highlighting the improvements are documented in Table 3.

Weighted Eikonal We explore the effects of different configurations of the Eikonal loss. Specifically, we compare our method using a standard Eikonal loss that is applied uniformly to all sample points with our adaptively weighted Eikonal loss. We observe that the standard Eikonal loss results in learned UDFs with lower accuracy near the zero level

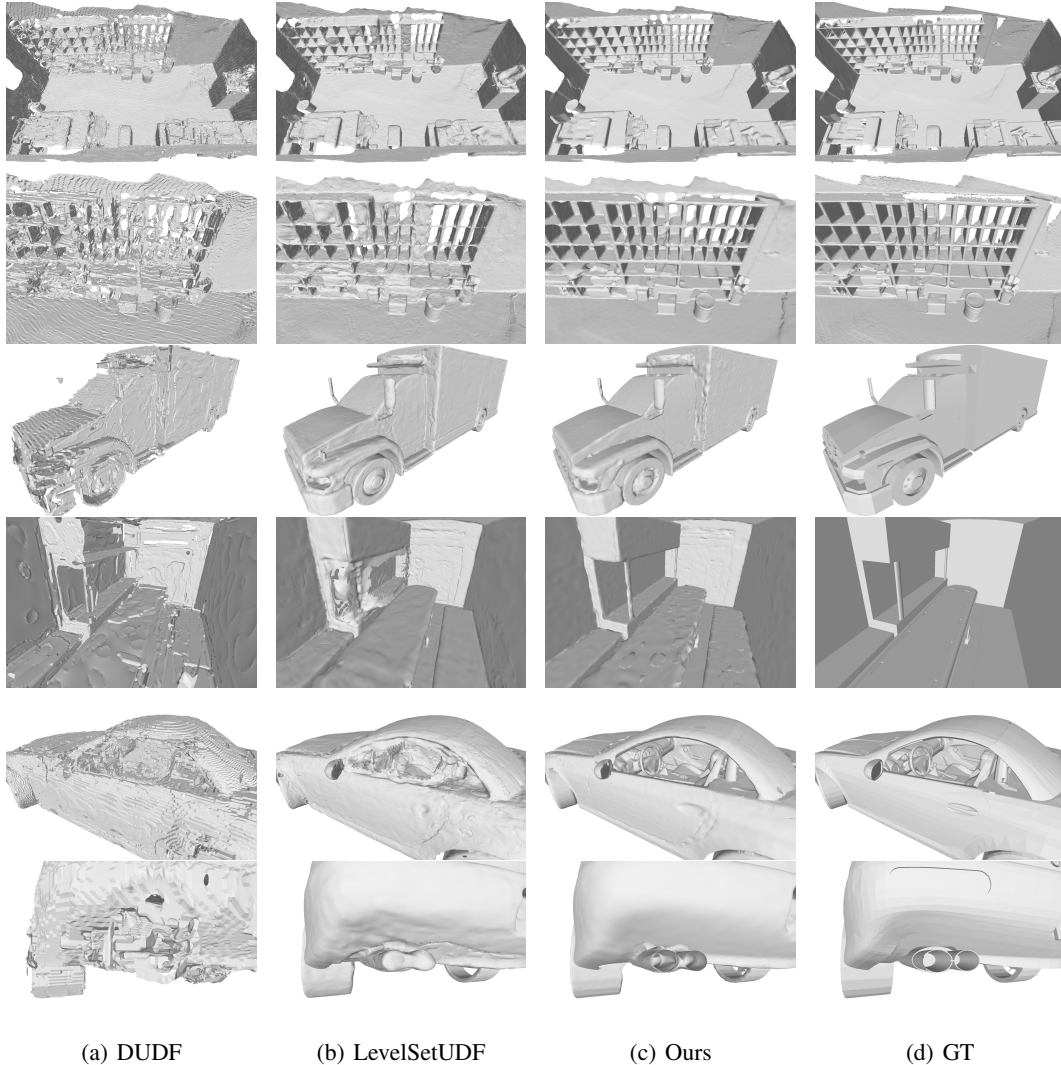


Figure 3: Visual comparison with DUDF and LevelSetUDF on an indoor scene from the Stanford 3D Scene dataset featuring noise and an imperfect scan, and two car models from the ShapeNet-Cars dataset showcasing complex inner structures. The open boundaries generated by our method are the best, such as, the building windows, inner structures of the vehicle and car exhaust vent.

Table 3: Ablation studies on the model “Stonewall” in the Stanford 3D Scene Dataset.

	CD-mean	CD-median	$F1^{0.01}$	$F1^{0.005}$
SIREN+Abs.	5.27	3.07	87.65	77.87
SIREN+softplus	2.91	2.71	99.79	91.08
w/o weighted Eikonal	2.87	2.54	99.26	90.98
w/o normal alignment	3.20	2.97	99.36	88.68
DEUDF	2.69	2.51	99.95	93.52

sets, leading to numerous small holes in the extracted meshes. In contrast, our adaptively weighted Eikonal loss more effectively address the issues of vanishing gradient, and stabilizes the learning process, thereby yielding meshes with higher quality. Due to the uniform Eikonal constraint obstructing the UDF learning process at the zero level set, slightly higher distance values are observed around the target surface. To accommodate these inaccuracies, we applied a higher threshold of 0.01, instead of the default value of 0.0025 used in DCUDF, for extracting the surface.

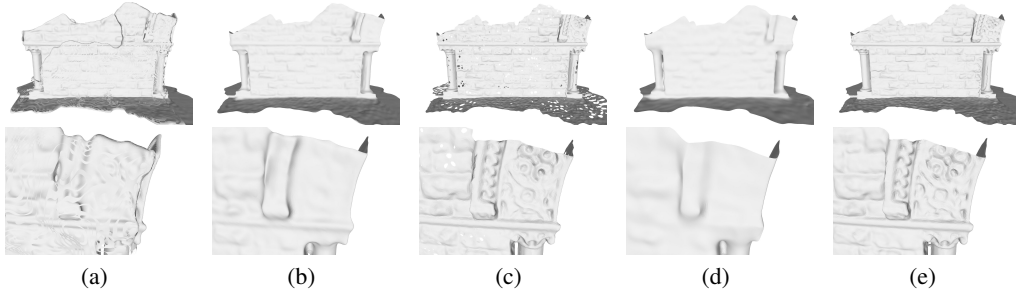


Figure 4: Visual results from the ablation studies: (a) Applying the absolute value to the output of the SIREN network. (b) Applying the softplus function to the output of the SIREN network. (c) Using uniform Eikonal constraints. (d) Removing normal alignment. (e) Applying all components.

5 Conclusions

This paper presents an improved UDF learning method for high fidelity 3D surface reconstruction. The method integrates novel UDF representation without absolute or softplus, normal alignment, adaptively weighted Eikonal constraint and SIREN network to learn more accurate UDFs. Our DEUDF can learn not only geometry details but also geometry boundaries, thereby maintaining better topology. Extensive experiments illustrate that our method produces low Chamfer distances and better topology outperforming state-of-the-art methods.

Since our method needs normals as guidance, the input point cloud should be dense. Moreover, to learn model details also needs dense input. In the future, we will investigate to learn uneven density point cloud, where the points are sparse in smooth regions and dense in detailed regions. Another limitation is highly noisy point clouds, which are challenge for detailed model learning. We will explore how to learn noise inputs in the future.

References

- [1] Benoit Guillard, Federico Stella, and Pascal Fua. Meshudf: Fast and differentiable meshing of unsigned distance field networks. In *Proc. of ECCV*, pages 576–592, 2022.
- [2] Julian Chibane, Aymen Mir, and Gerard Pons-Moll. Neural unsigned distance fields for implicit function learning. In *Proc. of NeurIPS*, pages 21638–21652, 2020.
- [3] Junsheng Zhou, Baorui Ma, Yu-Shen Liu, Yi Fang, and Zhizhong Han. Learning consistency-aware unsigned distance functions progressively from raw point clouds. In *Proc. of NeurIPS*, pages 16481–16494, 2022.
- [4] Junsheng Zhou, Baorui Ma, Shujuan Li, Yu-Shen Liu, and Zhizhong Han. Learning a more continuous zero level set in unsigned distance fields through level set projection. In *Proc. of ICCV*, pages 3158–3169, Los Alamitos, CA, USA, oct 2023. IEEE Computer Society.
- [5] Hugues Hoppe, Tony DeRose, Tom Duchamp, John McDonald, and Werner Stuetzle. Surface reconstruction from unorganized points. *SIGGRAPH Comput. Graph.*, 26(2):71–78, jul 1992.
- [6] Yu-Tao Liu, Li Wang, Jie Yang, Weikai Chen, Xiaoxu Meng, Bo Yang, and Lin Gao. NeUDF: Learning neural unsigned distance fields with volume rendering. In *Proc. of CVPR*, pages 237–247, 2023.
- [7] Vincent Sitzmann, Julien N. P. Martel, Alexander W. Bergman, David B. Lindell, and Gordon Wetzstein. Implicit neural representations with periodic activation functions. In *Proc. of NeurIPS*, Red Hook, NY, USA, 2020. Curran Associates Inc.
- [8] Fei Hou, Xuhui Chen, Wencheng Wang, Hong Qin, and Ying He. Robust zero level-set extraction from unsigned distance fields based on double covering. *ACM Trans. Graph.*, 42(6), 2023.

- [9] Nina Amenta and Marshall Bern. Surface reconstruction by voronoi filtering. In *Proceedings of SoCG*, pages 39–48, 1998.
- [10] Tamal K. Dey and Samrat Goswami. Tight cocone: A water-tight surface reconstructor. In *Proc. of ACM SMA*, pages 127–134, 2003.
- [11] Yutaka Ohtake, Alexander Belyaev, Marc Alexa, Greg Turk, and Hans-Peter Seidel. Multi-level partition of unity implicits. *ACM Trans. Graph.*, 22(3):463–470, 2003.
- [12] Michael Kazhdan, Matthew Bolitho, and Hugues Hoppe. Poisson surface reconstruction. In *Proc. of SGP*, pages 61–70, 2006.
- [13] Fei Hou, Chiyu Wang, Wencheng Wang, Hong Qin, Chen Qian, and Ying He. Iterative poisson surface reconstruction (ipsr) for unoriented points. *ACM Trans. Graph.*, 41(4), 2022.
- [14] Jeong Joon Park, Peter Florence, Julian Straub, Richard Newcombe, and Steven Lovegrove. Deep sdf: Learning continuous signed distance functions for shape representation. In *Proc. of CVPR*, pages 165–174, 2019.
- [15] Siyu Ren, Junhui Hou, Xiaodong Chen, Ying He, and Wenping Wang. Geoudf: Surface reconstruction from 3d point clouds via geometry-guided distance representation. In *Proc. of ICCV*, pages 14214–14224, 2023.
- [16] Ruian Wang, Zixiong Wang, Yunxiao Zhang, Shuang-Min Chen, Shiqing Xin, Changhe Tu, and Wenping Wang. Aligning gradient and hessian for neural signed distance function. In Alice Oh, Tristan Naumann, Amir Globerson, Kate Saenko, Moritz Hardt, and Sergey Levine, editors, *NeurIPS*, 2023.
- [17] Miguel Fainstein, Viviana Silless, and Emmanuel Iarussi. DUDF: differentiable unsigned distance fields with hyperbolic scaling. In *Proc. of CVPR*, 2024.
- [18] Lars Mescheder, Michael Oechsle, Michael Niemeyer, Sebastian Nowozin, and Andreas Geiger. Occupancy networks: Learning 3d reconstruction in function space. In *CVPR*, pages 4455–4465, 2019.
- [19] Julian Chibane, Thiemo Alldieck, and Gerard Pons-Moll. Implicit functions in feature space for 3d shape reconstruction and completion. In *Proc. of CVPR*, pages 6968–6979, 2020.
- [20] Songyou Peng, Michael Niemeyer, Lars Mescheder, Marc Pollefeys, and Andreas Geiger. Convolutional occupancy networks. In *ECCV*, pages 523–540, 2020.
- [21] Rohan Chabra, Jan E. Lenssen, Eddy Ilg, Tanner Schmidt, Julian Straub, Steven Lovegrove, and Richard Newcombe. Deep local shapes: Learning local sdf priors for detailed 3d reconstruction. In *Proc. of ECCV*, pages 608–625, 2020.
- [22] Yifan Wang, Lukas Rahmann, and Olga Sorkine-Hornung. Geometry-consistent neural shape representation with implicit displacement fields. In *Proc. of ICLR*, 2022.
- [23] Peng Wang, Lingjie Liu, Yuan Liu, Christian Theobalt, Taku Komura, and Wenping Wang. Neus: Learning neural implicit surfaces by volume rendering for multi-view reconstruction. *NeurIPS*, 2021.
- [24] Lior Yariv, Jiatao Gu, Yoni Kasten, and Yaron Lipman. Volume rendering of neural implicit surfaces. In *Advances in Neural Information Processing Systems*, pages 4805–4815, 2021.
- [25] Jianglong Ye, Yuntao Chen, Naiyan Wang, and Xiaolong Wang. GIFS: Neural implicit function for general shape representation. In *Proc. of CVPR*, pages 12819–12829, 2022.
- [26] Xianghui Yang, Guosheng Lin, Zhenghao Chen, and Luping Zhou. Neural vector fields: Implicit representation by explicit learning. In *Proceedings of the IEEE/CVF Conference on Computer Vision and Pattern Recognition (CVPR)*, pages 16727–16738, June 2023.
- [27] Xiaoxiao Long, Cheng Lin, Lingjie Liu, Yuan Liu, Peng Wang, Christian Theobalt, Taku Komura, and Wenping Wang. NeuralUDF: Learning unsigned distance fields for multi-view reconstruction of surfaces with arbitrary topologies. In *Proc. of CVPR*, pages 20834–20843, 2023.
- [28] Junkai Deng, Fei Hou, Xuhui Chen, Wencheng Wang, and Ying He. 2s-udf: A novel two-stage udf learning method for robust non-watertight model reconstruction from multi-view images. In *Proc. of CVPR*, 2024.
- [29] Diederik P. Kingma and Jimmy Ba. Adam: A method for stochastic optimization. In *Proc. of ICLR*, 2015.
- [30] Ilya Loshchilov and Frank Hutter. SGDR: stochastic gradient descent with warm restarts. In *5th International Conference on Learning Representations, ICLR 2017, Toulon, France, April 24-26, 2017, Conference Track Proceedings*. OpenReview.net, 2017.
- [31] Zixiong Wang, Yunxiao Zhang, Rui Xu, Fan Zhang, Peng-Shuai Wang, Shuang-Min Chen, Shiqing Xin, Wenping Wang, and Changhe Tu. Neural-singular-hessian: Implicit neural representation of unoriented point clouds by enforcing singular hessian. *ACM Trans. Graph.*, 42(6):274:1–274:14, 2023.

- [32] Angel X. Chang, Thomas Funkhouser, Leonidas Guibas, Pat Hanrahan, Qixing Huang, Zimo Li, Silvio Savarese, Manolis Savva, Shuran Song, Hao Su, Jianxiong Xiao, Li Yi, and Fisher Yu. Shapenet: An information-rich 3d model repository, 2015.
- [33] Qian-Yi Zhou and Vladlen Koltun. Dense scene reconstruction with points of interest. *ACM Transactions on Graphics*, 32, 07 2013.

A Appendix

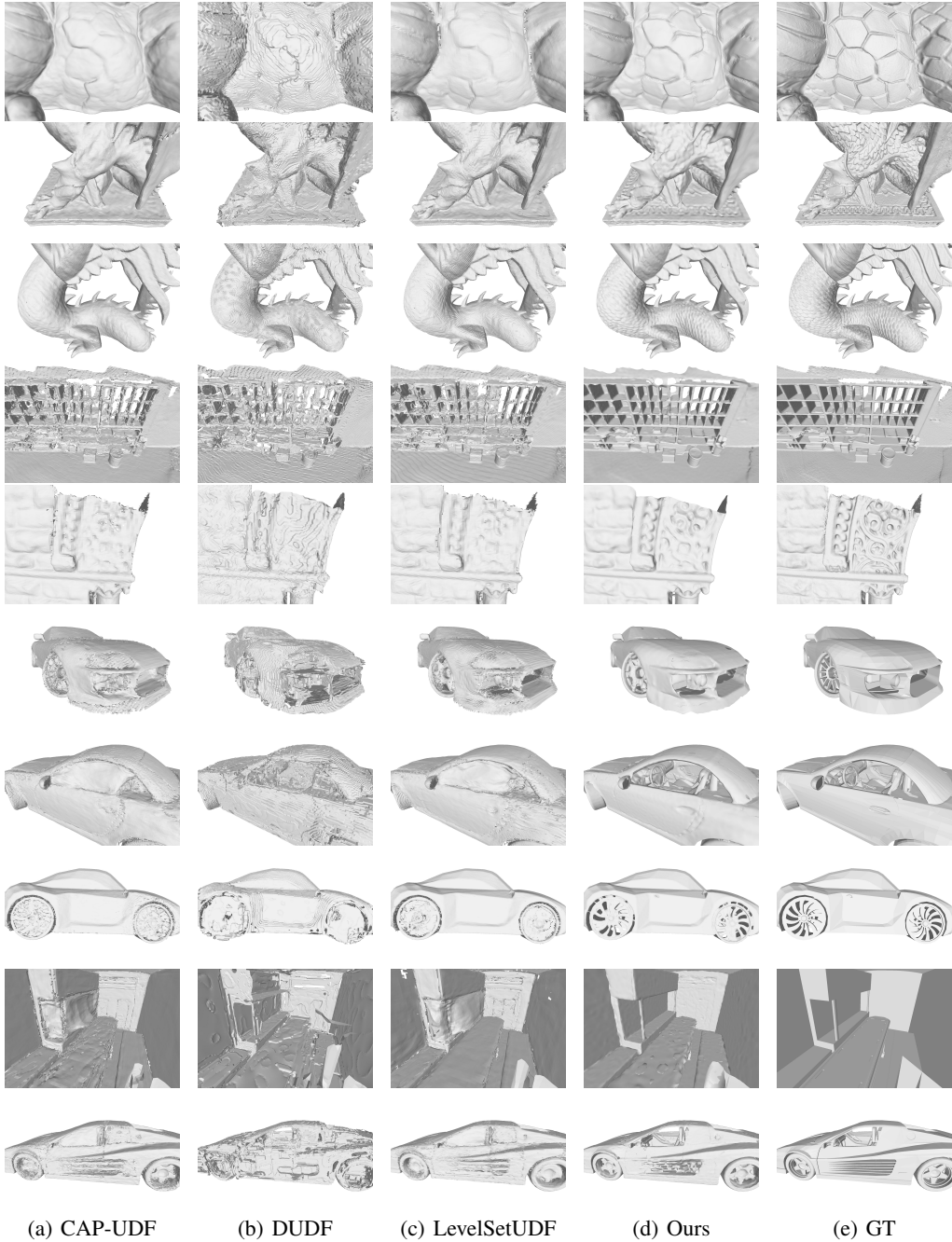


Figure 5: Visual comparison with CAP-UDF, DUDF, LevelSetUDF, and our DEUDF across various test models. To eliminate the impact of adopting DCUDF for extracting zero level sets from the learned UDF, we utilize the same zero level set extraction technique as originally proposed/used for each method. Still, our method consistently delivers results with higher quality, characterized by more detailed geometric features and smoother shape boundaries.

We present additional comparisons with CAP-UDF [3] and LevelSetUDF [4] by their original implementations as illustrated in Figure 5 and detailed in Table 4. The accuracy is lower than using DCUDF [8] for surface extraction. Our method produces higher quality results, characterized by enhanced geometric details and smoother shape boundaries. In Figure 6 and 7, we show more results for models with details and models with complex topology and inner structures.

The surfaces are all extracted by DCUDF except DUDF [17] by the original method. Our method outperforms DUDF, CAP-UDF and LevelSetUDF in terms of accuracy and topology.

Table 4: Quantitative comparisons with the original results of CAP-UDF and LevelSetUDF. Chamfer distances are measured in the unit of $\times 10^{-3}$. We randomly sampled 100K points from each ground truth mesh and then computed both CDs and F-scores as reference performance metrics. Therefore, the closer the actual performance metrics are to these references, the higher the quality of the results produced by the method.

		Stanford 3D Scene				Stanford 3D Scan				ShapeNet-Cars			
		Chamfer-L1 (\downarrow)		F-score (\uparrow)		Chamfer-L1 (\downarrow)		F-score (\uparrow)		Chamfer-L1 (\downarrow)		F-score (\uparrow)	
Method	Distance	Mean	Median	$F1^{0.01}$	$F1^{0.005}$	Mean	Median	$F1^{0.01}$	$F1^{0.005}$	Mean	Median	$F1^{0.01}$	$F1^{0.005}$
CAP-UDF	Unsigned	3.32	3.12	99.36	84.98	4.11	3.87	99.12	69.24	4.95	4.67	95.49	55.9
LevelSetUDF	Unsigned	3.16	2.93	99.32	85.90	4.10	3.85	99.13	69.42	5.07	4.76	94.98	54.30
Ours	Unsigned	3.09	2.85	99.41	86.38	4.08	3.83	99.14	69.59	4.91	4.58	95.53	56.98

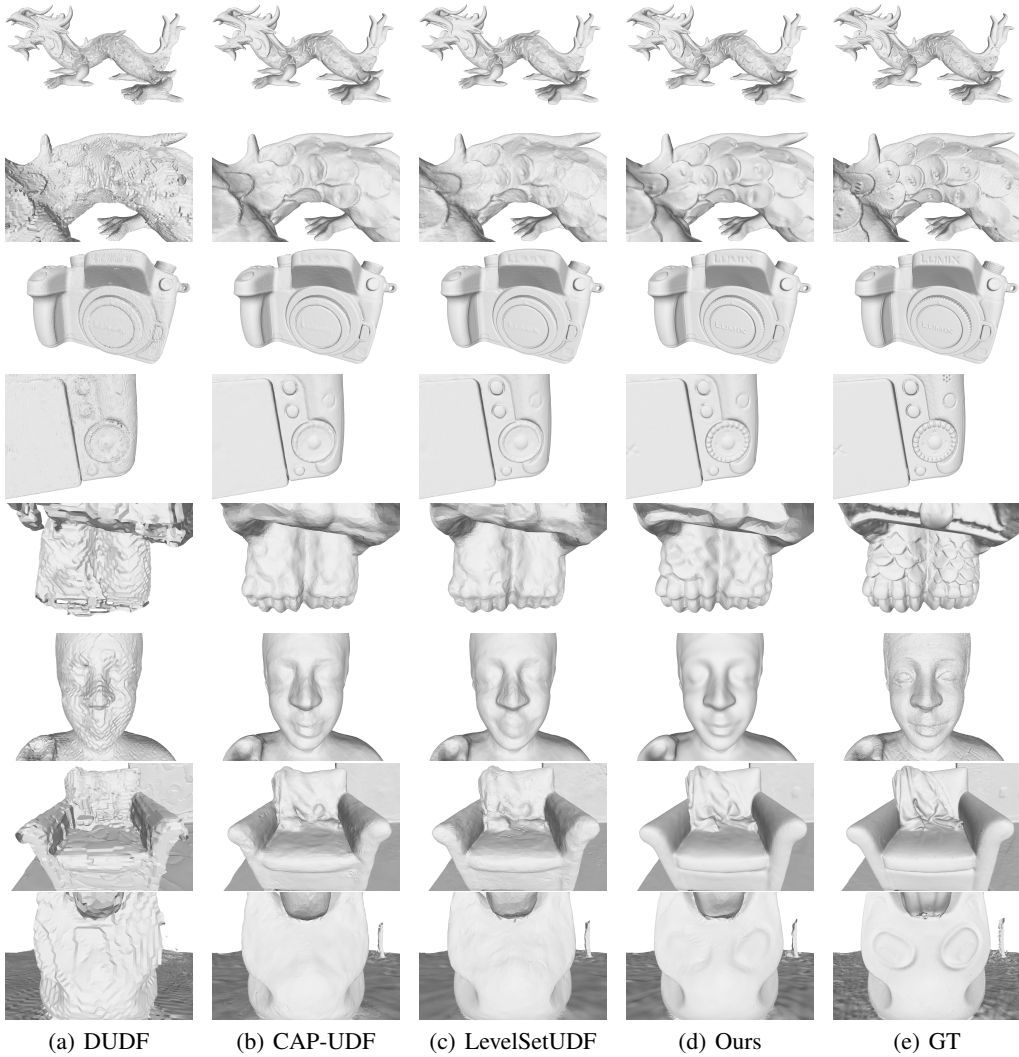


Figure 6: More visual comparisons with DUDF, CAPUDF and LevelSetUDF on detailed models from the Stanford 3D Scan dataset and Stanford 3D Scene dataset. Our method learns more details.

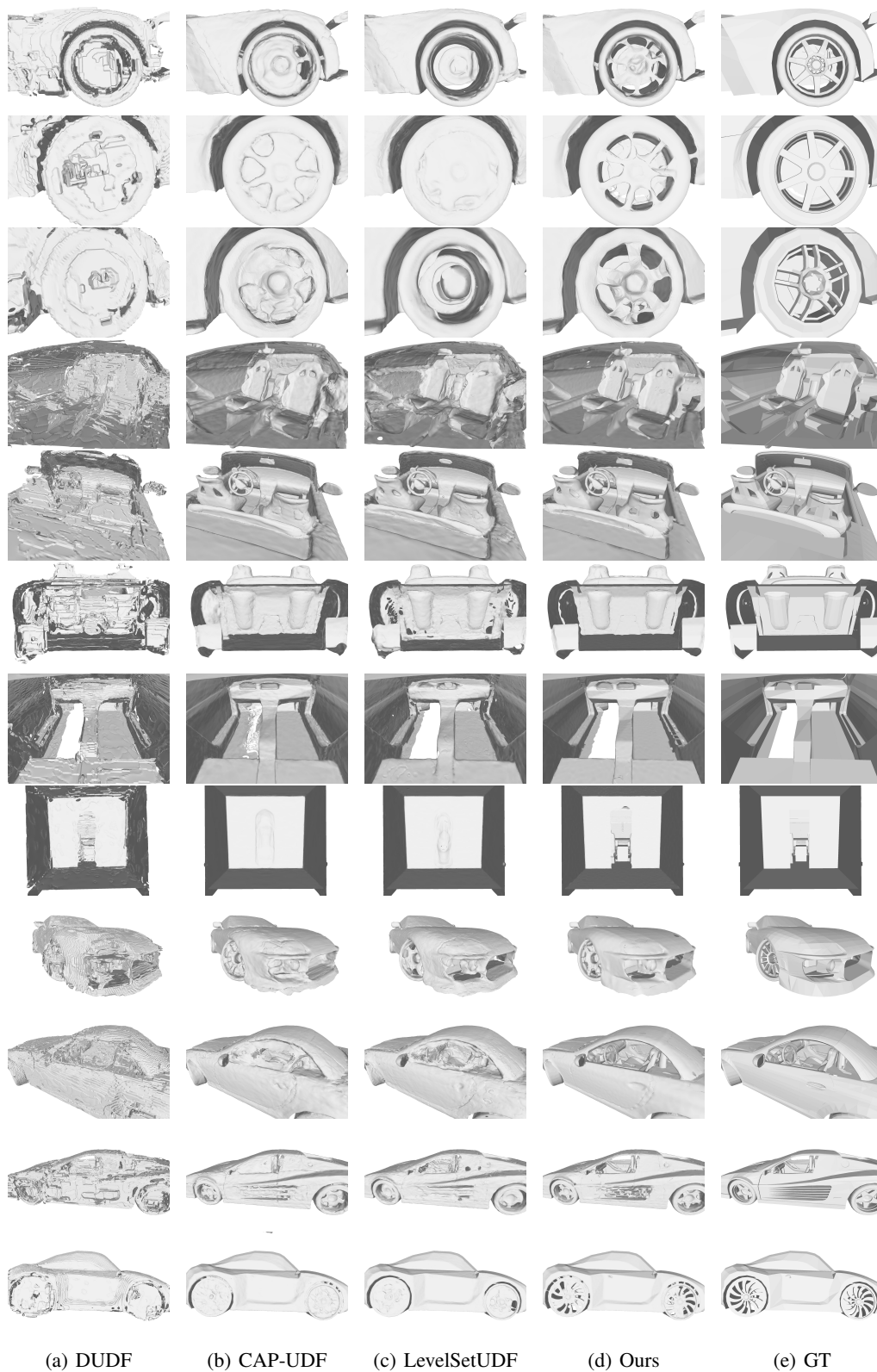


Figure 7: More visual comparisons with DUDF, CAPUDF and LevelSetUDF on car models from the ShapeNet-Cars dataset showcasing better reconstruction for complex inner structures.